Native Frames: Disentangling Sequential from Concerted Three-Body Fragmentation

Jyoti Rajput, T. Severt, Ben Berry, Bethany Jochim, Peyman Feizollah, Balram Kaderiya, M. Zohrabi, U. Ablikim, Farzaneh Ziaee, Kanaka Raju P., D. Rolles, A. Rudenko, K. D. Carnes, B. D. Esry, and I. Ben-Itzhak

Phys. Rev. Lett. **120**, 103001 — Published 8 March 2018

DOI: 10.1103/PhysRevLett.120.103001

Native frames: Disentangling sequential from concerted three-body fragmentation

Jyoti Rajput,* T. Severt, Ben Berry, Bethany Jochim, Peyman Feizollah, Balram Kaderiya, M. Zohrabi, U. Ablikim, Farzaneh Ziaee, Kanaka Raju P., D. Rolles, A. Rudenko, K. D. Carnes, B. D. Esry, and I. Ben-Itzhak†
J. R. Macdonald Laboratory, Physics Department,
Kansas State University, Manhattan, Kansas 66506
(Dated: January 22, 2018)

A key question concerning three-body fragmentation of polyatomic molecules is the distinction of sequential and concerted mechanisms, i.e., the stepwise or simultaneous cleavage of bonds. Using laser-driven fragmentation of OCS into $O^+ + C^+ + S^+$ and employing coincidence momentum imaging, we demonstrate a novel method that enables clear separation of sequential and concerted breakup. The separation is accomplished by analyzing the three-body fragmentation in the native frame associated with each step and taking advantage of the rotation of the intermediate molecular fragment, CO^{2+} or CS^{2+}, before its unimolecular dissociation. This native-frame method works for any projectile (electrons, ions, or photons), provides details on each step of the sequential breakup, and enables the retrieval of the relevant spectra for sequential and concerted breakup separately. Specifically, this allows the determination of the branching ratio of all these processes in OCS^{3+} breakup. Moreover, we find that the first step of sequential breakup is tightly aligned along the laser polarization and identify the likely electronic states of the intermediate dication that undergo unimolecular dissociation in the second step. Finally, the separated concerted breakup spectra show clearly that the central carbon atom is preferentially ejected perpendicular to the laser field.

Advances in imaging techniques have led to better understanding of molecular fragmentation [1–6]. Experimentally distinguishing between concerted and sequential (sometimes called stepwise) fragmentation mechanisms in polyatomic molecules is a long-standing goal of these efforts (see, for example, [3, 5, 7–17]). Key to its achievement is the coincidence detection of all fragments, although alternatives without coincidence measurements have been suggested [7]. In recent years, coincidence momentum imaging techniques have progressed significantly toward this goal [5, 10–17].

Despite these advances, understanding three-body breakup remains a challenge. For instance, one process that still requires work is the sequential three-body breakup of a triatomic molecule. In the case of a triply-charged triatomic, which can be imaged easily, there may be an intermediate step. Of particular interest are metastable intermediate states that survive much longer than their rotational period, i.e., $\tau \gg T_R$. This sequential process has been invoked to explain a circular feature in a Newton diagram showing the momentum correlation of the three final fragments measured in coincidence [5, 12–14, 16, 17]. The same fragmentation mechanism appears as a linear distribution across a Dalitz plot [5, 12–16] — a plot depicting the energy sharing among the three fragments [18]. However, neither of these data visualization strategies facilitates complete separation of sequential fragmentation and concerted breakup.

One step towards resolving this problem was taken in a recent study of core-hole localization by Guillemin *et al.* [13]. They managed to partly separate $CS_2^{4+} \rightarrow C^+ + S^+ + S^{2+}$ fragmentation events associated with the sequential or concerted mechanisms. Though the separation was sufficient to address the question of core localization versus delocalization, they stated clearly the limitations of their method, saying, "because the disentanglement of the two fragmentation mechanisms is based solely on kinetic energy considerations, this selection is imperfect and both mechanisms can still contribute moderately to the resulting" spectra.

In this work, we demonstrate a more complete way to analyze three-body breakup data that allows us to systematically distinguish sequential fragmentation events as long as the intermediate molecule rotates long enough.

The beauty of the method presented here is that it also allows us to "recover" sequential fragmentation events that are masked by competing processes, and therefore enables generation of spectra for concerted breakup events through subtraction of the sequential fragmentation events.

To demonstrate our method, we use triple ionization of OCS leading to $O^+ + C^+ + S^+$, because two sequential fragmentation routes, proceeding through $S^+ + CO^{2+}$ or $O^+ + CS^{2+}$, have been reported [14]. The events identified with each sequential breakup mechanism reveal essential information that enables one to pinpoint the intermediate states of the diatomic dication as well as the precursor OCS^{3+} states involved in the dissociation path. Moreover, the separation of these sequential fragmentation channels from each other and from the concerted breakup facilitates branching ratios determination.

In our experiment, triple ionization of OCS was initiated by intense ($\lesssim 10^{15}\,\mathrm{W/cm^2}$) linearly-polarized ($\boldsymbol{E} \| \boldsymbol{Z}$) laser pulses centered at 790 nm with 23-fs duration (FWHM in intensity) provided at 10 kHz by our PULSAR laser [19]. The laser was focused on a supersonic jet within a COLTRIMS apparatus [20] (see reviews [21–23]), where the time-of-flight (TOF) and position information of each ion is recorded event-by-event. The primary channel of interest is the fragmentation of OCS^{3+}

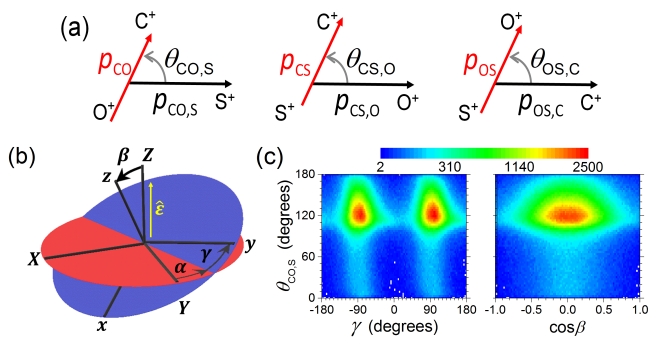

FIG. 1. (Color online) (a) Relative momenta of three-body breakup, where the black and red arrows represent the first and second breakup steps with the angle $\theta_{\mathrm{AB,C}}$ in between — all labeled by the relevant fragments ($\theta_{\mathrm{AB,C}}$ is a polar angle in the body frame). (b) The Euler angles [25] of the fragmentation plane (blue) [26] for sequential breakup via $CO^{2+}+S^{+}$. (c) All $O^{+}+C^{+}+S^{+}$ events as a function of $\theta_{\mathrm{CO,S}}$ and γ or $\cos\beta$ (integrated over the other angles).

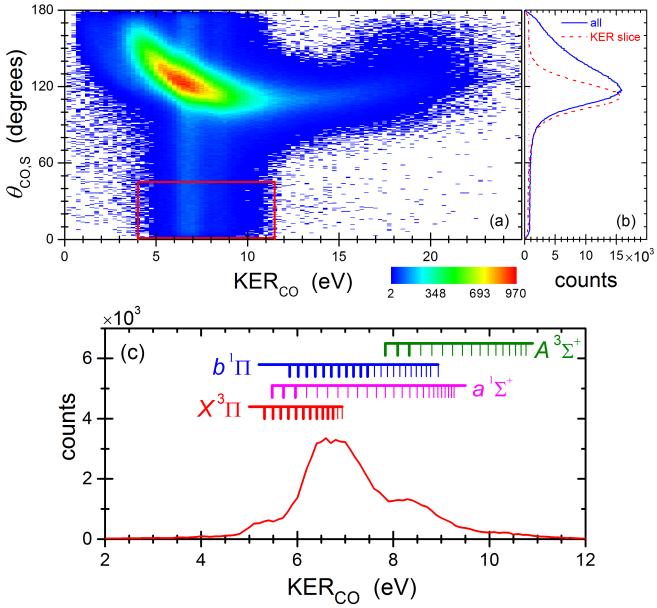

FIG. 2. (Color online) Sequential breakup of OCS^{3+} via $CO^{2+}+S^{+}$. (a) A density plot of $O^{+}+C^{+}+S^{+}$ events as a function of $\mathrm{KER_{CO}}$ and $\theta_{\mathrm{CO,S}}$. The gate used to select the sequential breakup events is marked as a red box. (b) The $N(\theta_{\mathrm{CO,S}})$ distributions for all events (solid-blue line) and events within a $\mathrm{KER_{CO}}$ slice 8–11 eV (dashed-red line), matched at the peak. The KER slice indicates that the flat distribution extends to small angles. (c) $\mathrm{KER_{CO}}$ distribution of CO^{2+} unimolecular dissociation (step 2) for events within $\theta_{\mathrm{CO,S}}=[0°,45°]$. The tick marks indicate the expected KER values for field free J=1 states (see text).

into $O^{+}+C^{+}+S^{+}$ identified by triple coincidence [24]. We also measured the two-body breakup channels associated with sequential fragmentation, namely $S^{+}+CO^{2+}$ and $O^{+}+CS^{2+}$, for which the metastable dication's lifetime is longer than its TOF.

The first challenge is to identify which $O^{+}+C^{+}+S^{+}$ events result from sequential fragmentation. Classically, what sets these events apart is that the intermediate molecular fragment rotates long enough to "forget" any alignment imprinted by the first breakup step [5, 12–16]. However, instead of using a Newton diagram or Dalitz plot to identify these events, we take advantage of the two-step nature of the process and analyze the data in the two native frames of reference associated with each breakup step. Specifically, we analyze the first step in the OCS^{3+} center-of-mass (CM) frame and the second step in the CM frame of the intermediate dication, using the relative momenta, shown in Fig. 1(a), defined from the three-body Jacobi coordinates (see, e.g., Refs. [27, 28]).

Importantly, the relative direction of the CO^{2+} unimolecular dissociation in the fragmentation plane, denoted by the angle $\theta_{\mathrm{CO,S}}$ in Fig. 1(a), is intuitively expected to be uniform for states that rotate long compared to the rotational period. Since classical calculations indicate that the Coulomb repulsion can impart high angular momentum ($\sim 60\,\hbar$) to the CO^{2+} [5, 29] the relevant rotational period can be considerably shorter than expected for J=1. The calculations also suggest that this rotation occurs in the molecular plane [30].

In cases where such modeling is not feasible, however, we can directly test whether the CO^{2+} rotates in the fragmentation plane using the Euler angles defined in Fig. 1(b). The Euler-angle distributions shown in Fig. 1(c) reveal, for example, that three-body breakup is favored when the laser polarization is in the fragmentation plane, $\cos\beta=0$. Because of this, the peaks at $\gamma=\pm 90°$ indicate a clear preference for the first breakup step to align with the laser field. Most importantly, though, the flat ridges visible for $\theta_{\mathrm{CO,S}}<100°$ indicate that $N(\theta_{\mathrm{CO,S}})$ is constant as expected if the CO^{2+} rotates in the fragmentation plane independent of the plane's alignment. The constant $N(\theta_{\mathrm{CO,S}})$ distribution is the signature used to identify sequential breakup events not masked by other competing processes, and is employed to "recover" concealed sequential events. Notice that although $\theta_{\mathrm{AB,C}}$ is a polar angle, $N(\theta_{\mathrm{AB,C}})$ is uniform as befits rotation in a plane—the more usual $N(\cos\theta_{\mathrm{AB,C}})$ would be isotropic for rotation on a sphere [30].

Another measurable that helps identify sequential fragmentation is the kinetic energy release (KER) in the second step [31, 32], i.e., $\mathrm{KER_{CO}} = p_{\mathrm{CO}}^{2}/2\mu_{\mathrm{CO}}$, where p_{CO} and μ_{CO} are, respectively, the relative momentum and reduced mass of the C^{+} and O^{+} fragments. Note that $\mathrm{KER_{CO}}$ is expected to enable identification of the metastable states of CO^{2+} playing a role.

We plot all the $O^{+}+C^{+}+S^{+}$ events as a function of $\mathrm{KER_{CO}}$ and $\theta_{\mathrm{CO,S}}$ in Fig. 2(a). The sequential fragmentation proceeding through a CO^{2+} intermediate molecule is clearly identified as the uniform angular distribution cen-

tered around 6.5 eV. The dominant concerted breakup channel peaks around $(\mathrm{KER}_{\mathrm{CO}}, \theta_{\mathrm{CO,S}}) = (6.3\,\mathrm{eV}, 120°)$ leaving a wide range of $\theta_{\mathrm{CO,S}}$ where sequential fragmentation events can be observed as the expected flat $N(\theta_{\mathrm{CO,S}})$ distribution. This flat distribution extends over the whole $\theta_{\mathrm{CO,S}}$ range and becomes visible again for $\theta_{\mathrm{CO,S}}$ approaching 180° as illustrated in Fig. 2(b). We note that the narrow dips in $N(\theta_{\mathrm{CO,S}})$ around 0° and 180° are experimental artifacts caused by reduced detection efficiency near the detector center due to a high ion rate of OCS^{q+} and He ions from the carrier gas [30].

The unimolecular dissociation of CO^{2+} occurs mainly by predissociation due to spin-orbit coupling to the repulsive lowest $^3\Sigma^-$ state [33] on the μs to ps timescale, i.e. long after the laser pulse, and yields the $\mathrm{KER}_{\mathrm{CO}}$ distribution shown in Fig. 2(c). Similar KER spectra have been extensively used to identify possible states of dissociating diatomic molecules (e.g., Refs. [34, 35]).

The KER of specific electronic and vibrational states of CO^{2+}, shown as thick tick marks in Fig. 2(c), are based on high-precision measurements of most of the low-lying metastable states [36], although a few KER were evaluated using measured vertical photo-ionization energies [37, 38]. We also calculated the KER of higher vibrational states with J=1 (thin tick marks) using the potentials from Ref. [33] and a phase-amplitude method [39]. The possible states can thus be identified by matching the KER values. For example, the peak of the measured $\mathrm{KER}_{\mathrm{CO}}$ distribution aligns well with the $X\,^3\Pi(v$=7–12) and $b\,^1\Pi(v$=3–6) states, and the low-energy shoulder matches the $a\,^1\Sigma^+(v$=0–2) and $X\,^3\Pi(v$=0–4) states, while the high-KER shoulder may have contributions from the $A\,^3\Sigma^+(v$=0–3) states.

The lifetimes of these states are also crucial to the interpretation of the data, as they must lie between the rotational period and a few-nanosecond maximum imposed by the imaging setup [40]. The relevant rotation period depends on the angular momentum imparted to the CO^{2+} in the first breakup step. Lifetimes calculated including the angular-momentum dependence [41, 42] suggest that many of the ro-vibrational states have lifetimes of the order of 100 ps and therefore can contribute to the $\mathrm{KER}_{\mathrm{CO}}$ spectrum shown in Fig. 2(c). As an illustration, we calculated pre-dissociation rates for $J = 1$ (see method in Ref. [43]), which suggest that the $X\,^3\Pi\,(v$=2,5,8,9) states have the right lifetimes (287, 35.8, 97.7, and 22 ps, respectively) to be key players in the measured sequential fragmentation. In contrast, the lifetime of the (v, J)=(4,1) state is below 1 ps and therefore may be too short to contribute. Clearly, further work is needed to pinpoint the importance of specific states.

The other sequential fragmentation, involving breakup into $\mathrm{O}^+ + \mathrm{CS}^{2+}$ in the first step, is analyzed similarly. In this case, we plot all $\mathrm{O}^+ + \mathrm{C}^+ + \mathrm{S}^+$ events as a function of $\mathrm{KER}_{\mathrm{CS}}$ and $\theta_{\mathrm{CS,O}}$ (defined in Fig. 1) in Fig. 3. Here also, a uniform angular distribution is observed for sequential

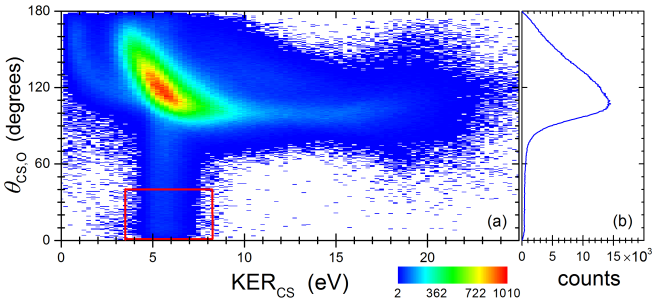

FIG. 3. (Color online) Sequential breakup of OCS^{3+} via $\mathrm{CS}^{2+} + \mathrm{O}^+$. (a) A density plot of $\mathrm{O}^+ + \mathrm{C}^+ + \mathrm{S}^+$ as a function of $\mathrm{KER}_{\mathrm{CS}}$ and $\theta_{\mathrm{CS,O}}$. The gate used to select the sequential breakup events is marked by a red box. (b) The $N(\theta_{\mathrm{CS,O}})$ distribution for all events.

fragmentation events with a CS^{2+} intermediate enabling their selection. Like the other sequential channel, the $\mathrm{KER}_{\mathrm{CS}}$ distribution and lifetimes of the CS^{2+} states can be used to identify the dissociation path [30].

We return our attention to the first step of the sequential fragmentation and explore its alignment with respect to the laser field, denoted by the angle θ between the polarization and the atomic fragment momentum. The other measurable is the first-step KER [32], given by $\mathrm{KER}_{\mathrm{CO,S}} = p^2_{\mathrm{CO,S}}/(2\mu_{\mathrm{CO,S}})$, where $1/\mu_{\mathrm{CO,S}} = 1/m_{\mathrm{CO}} + 1/m_{\mathrm{S}}$ and $m_{\mathrm{CO}} = m_{\mathrm{C}} + m_{\mathrm{O}}$, for $\mathrm{S}^+ + \mathrm{CO}^{2+} \rightarrow \mathrm{O}^+ + \mathrm{C}^+ + \mathrm{S}^+$ breakup, with similar expressions for breakup via $\mathrm{O}^+ + \mathrm{CS}^{2+}$.

In Fig. 4 we compare the fragmentation events identified as sequential (3-body) to those for which the metastable dication created in step 1 remained intact all the way to the detector (2-body). Note the similarity between the final $\mathrm{KER}_{\mathrm{CO,S}}$–$\cos\theta$ maps of the 2- and 3-body sequential breakup channels, both tightly aligned along

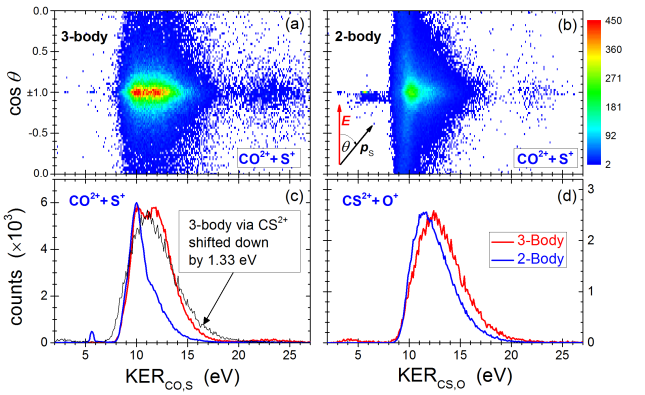

FIG. 4. (Color online) First step of OCS^{3+} sequential fragmentation. Yield of $\mathrm{CO}^{2+} + \mathrm{S}^+$ as a function of $\mathrm{KER}_{\mathrm{CO,S}}$ and $\cos\theta$ for (a) three-body and (b) two-body breakup. Yield of (c) $\mathrm{CO}^{2+} + \mathrm{S}^+$ and (d) $\mathrm{CS}^{2+} + \mathrm{O}^+$ as a function of KER (scaled by peak height).

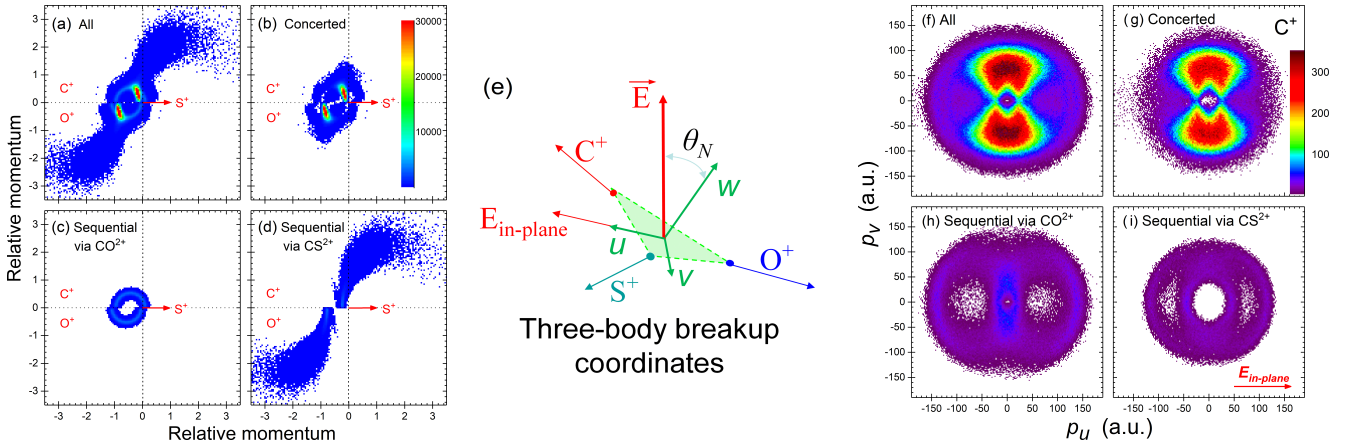

FIG. 5. (Color online) Channel separation, where "All" denotes all channels together, while "Concerted," "Sequential via CO^{2+}," and "Sequential via CS^{2+}," refer to the separate breakup channels, respectively (see text). (a-d) Newton diagrams showing relative momenta with respect to S^+ momentum, which is set along the x-axis. (e) The u, v three-body fragmentation plane where u is parallel to the polarization projection in this plane. (f-i) Momentum distribution of the C^+ fragment in the fragmentation plane.

the laser polarization. Interestingly, $\mathrm{KER}_{\mathrm{CO,S}}$ is lower than $\mathrm{KER}_{\mathrm{CS,O}}$ by about 1.33 eV — the energy difference between the two dissociation limits [as demonstrated by the shifted $O^+ + CS^{2+}$ distribution (black line) in Fig. 4(c)]. This suggests that both sequential fragmentation channels have the same excitation energy, thus involving the same group of OCS^{3+} potentials.

In addition to the detailed information on sequential fragmentation discussed above, this method allows the determination of the branching ratio of sequential and concerted breakup channels. Taking advantage of the uniform $N(\theta_{\mathrm{CO,S}})$ distribution, the total number of events in each sequential fragmentation channel leading to $O^+ + C^+ + S^+$ is simply given by $[180\,/\,(\theta_{max} - \theta_{min})]\ \Sigma_{\theta_{min}}^{\theta_{max}} N(\theta_{\mathrm{CO,S}})$ [44], where $[\theta_{min}, \theta_{max}]$ is the gate set on Figs. 2(a) and 3(a). The number of concerted events is then evaluated by subtracting the sequential ones from the total. The branching ratios of the $O^+ + C^+ + S^+$, $S^+ + CO^{2+}$ and $O^+ + CS^{2+}$ channels in the concerted and first step of sequential breakup are $0.699{\pm}0.007 : 0.199{\pm}0.008 : 0.102{\pm}0.006$, respectively. In the second step, 86.9±3.7 % and 80.0±5.0 % of the CO^{2+} and CS^{2+}, respectively, dissociate while the rest are detected intact in our measurement [30]. One may intuitively attribute the higher fraction of CO^{2+} over CS^{2+} production in step 1 to the "weaker" C–S bond in OCS [45], but that is not sufficient to explain why CO^{2+} production is approximately double that of CS^{2+}. Deeper understanding of the OCS^{3+} fragmentation in a strong field is needed to address this question.

We now demonstrate a unique additional strength of our Native-Frames method by separating the different fragmentation channels even where they overlap. This goal is accomplished by taking advantage of the expected flat $N(\theta_{\mathrm{CO,S}})$ distribution of the second fragmentation step when analyzed in the CM frame of the intermediate dication. Explicitly, for each event identified as sequential fragmentation with $\theta_{\mathrm{CO,S}}$ within the red "gate" in Fig. 2(a), we create an equivalent event by rotating it to a randomly generated $\theta_{\mathrm{CO,S}}$, $\theta'_{\mathrm{CO,S}}$, outside of the gate. This process is repeated until the distributions outside and inside the gate have the same average value $\overline{N(\theta_r)} = \overline{N(\theta_{\mathrm{CO,S}})}$ (see Ref. [30] for details).

Once a complete set of events for each sequential fragmentation channel is generated, their contributions can be subtracted from any desired spectrum containing all events to yield a separate concerted-breakup spectrum. This is demonstrated by a few examples in Fig. 5 (and Ref. [30]) and the discussion highlighting the information revealed by channel separation.

Newton diagrams for breakup through $S^+ + CO^{2+}$ and its separation into the individual fragmentation processes are shown in Fig. 5(a–d). Although diagrams like the one shown in panel (a) allowed the qualitative identification of sequential fragmentation via the circular feature [5, 12–14, 16], employing them for quantitative studies is limited. In contrast, the Native-Frames method enables channel separation, as shown in panels (b–d), and their quantitative exploration. We also note in panel (d) the high-momentum, "sprinkler-like," distribution caused by the other sequential breakup channel.

Finally, the momentum distribution of C^+ fragments in the fragmentation plane is shown in Fig. 5(f) in the common way. Subtracting the sequential channels reveals that only the dominant perpendicular component survives [see Fig. 5(g)], clearly indicating that in concerted breakup the central atom of the linear molecule

is preferentially ejected perpendicular to the laser field. The "circular" patterns in panels (h,i), which complicate the interpretation of the momentum image in Fig. 5(f), are caused by the fact that the fragmentation plane, defined by the relative momenta, is not directly correlated with the laser polarization because the second step occurs long after the laser pulse.

To summarize, we have introduced a powerful Native-Frames method to analyze three-body breakup, which allows one to identify sequential breakup if the intermediate molecular fragment rotates long enough to generate a uniform angular distribution in its CM frame. The key idea is to analyze the coincidence three-dimensional momentum imaging data in the native frame of reference associated with each breakup step and take advantage of the expected uniform $\theta_{\mathrm{AB,C}}$ distribution. This method provides detailed information about the two steps of sequential breakup, and it also allows the determination of the branching ratios of the competing breakup mechanisms, which is not easy with other methods.

Significantly, the simplicity of the KER–$\theta_{\mathrm{AB,C}}$ distribution facilitates the retrieval of all the sequential fragmentation events including those masked by other breakup channels. This enables their subtraction, allowing the concerted breakup spectra to be isolated.

This powerful method is not limited to the OCS molecule nor to laser-driven fragmentation. It should also be applicable to molecular three-body breakup of other charge states, including neutrals, and to more than three fragments. The principle of using the native frame for analysis applies in all these cases and more.

The specific advantages described here, however, require a sequential process in which the intermediate state has an identifiable property, such as sufficient angular momentum to generate a uniform angular distribution, to allow its separation. In the present case — as it will be in most cases — this property is assumed. It is a crucial feature of our method that this assumption can be tested. Specifically, we verify that the intermediate molecular fragment rotates preferentially in the fragmentation plane generating a uniform $\theta_{\mathrm{AB,C}}$ distribution that is independent of the alignment of that plane.

We thus expect the Native-Frames method to benefit future studies of breakup processes as well as the reanalysis of past measurements.

This work is supported by the Chemical Sciences, Geosciences, and Biosciences Division, Office of Basic Energy Sciences, Office of Science, U.S. Department of Energy under Award # DE-FG02-86ER13491.

* Presently at Department of Physics and Astrophysics, University of Delhi, Delhi 110007, INDIA.
† ibi@phys.ksu.edu

[1] B. Whitaker, ed., *Imaging in Molecular Dynamics – Technology and applications* (Cambridge University Press, New York, NY, 2003).
[2] J. Ullrich, ed., *Ten years of COLTRIMS and Reaction Microscopes* (Max-Planck-Institut fur Kernpysik Heidelberg, Heidelberg, Germany, 2004).
[3] U. Werner, K. Beckord, J. Becker, and H. O. Lutz, Phys. Rev. Lett. **74**, 1962 (1995).
[4] A. Hishikawa, A. Iwamae, and K. Yamanouchi, Phys. Rev. Lett. **83**, 1127 (1999).
[5] N. Neumann, D. Hant, L. P. H. Schmidt, J. Titze, T. Jahnke, A. Czasch, M. S. Schöffler, K. Kreidi, O. Jagutzki, H. Schmidt-Böcking, and R. Dörner, Phys. Rev. Lett. **104**, 103201 (2010).
[6] I. Bocharova, R. Karimi, E. F. Penka, J.-P. Brichta, P. Lassonde, X. Fu, J.-C. Kieffer, A. D. Bandrauk, I. Litvinyuk, J. Sanderson, and F. m. c. Légaré, Phys. Rev. Lett. **107**, 063201 (2011).
[7] C. E. M. Strauss and P. L. Houston, J. Chem. Phys. **94**, 8751 (1990).
[8] C. Maul and K.-H. Gericke, International Reviews in Physical Chemistry **16**, 1 (1997).
[9] S. Hsieh and J. H. D. Eland, Journal of Physics B: Atomic, Molecular and Optical Physics **30**, 4515 (1997).
[10] A. Hishikawa, H. Hasegawa, and K. Yamanouchi, Chemical Physics Letters **361**, 245 (2002).
[11] J. D. Savee, V. A. Mozhayskiy, J. E. Mann, A. I. Krylov, and R. E. Continetti, Science **321**, 826 (2008).
[12] C. Wu, C. Wu, D. Song, H. Su, Y. Yang, Z. Wu, X. Liu, H. Liu, M. Li, Y. Deng, Y. Liu, L.-Y. Peng, H. Jiang, and Q. Gong, Phys. Rev. Lett. **110**, 103601 (2013).
[13] R. Guillemin, P. Decleva, M. Stener, C. Bomme, T. Marin, L. Journel, T. Marchenko, R. Kushawaha, K. Jänkälä, N. Trcera, K. Bowen, D. Lindle, M. Piancastelli, and M. Simon, Nat. Comm. **6**, 6166 (2015).
[14] B. Wales, È. Bisson, R. Karimi, S. Beaulieu, A. Ramadhan, M. Giguère, Z. Long, W.-K. Liu, J.-C. Kieffer, F. Légaré, and J. Sanderson, J. Elect. Spectr. Rel. Phenom. **195**, 332 (2014).
[15] A. Ramadhan, B. Wales, R. Karimi, I. Gauthier, M. MacDonald, L. Zuin, and J. Sanderson, Journal of Physics B: Atomic, Molecular and Optical Physics **49**, 215602 (2016).
[16] Z. Shen, E. Wang, M. Gong, X. Shan, and X. Chen, The Journal of Chemical Physics **145**, 234303 (2016).
[17] X. Ding, M. Haertelt, S. Schlauderer, M. S. Schuurman, A. Y. Naumov, D. M. Villeneuve, A. R. W. McKellar, P. B. Corkum, and A. Staudte, Phys. Rev. Lett. **118**, 153001 (2017).
[18] R. Dalitz, The London, Edinburgh, and Dublin Philosophical Magazine and Journal of Science **44**, 1068 (1953).
[19] X. Ren, A. Summers, Kanaka-Raju P., A. Vajdi, V. Makhija, C. W. Fehrenbach, N. G. Kling, K. J. Betsch, Z. Wang, M. F. Kling, K. D. Carnes, I. Ben-Itzhak, C. Trallero-Herrero, and V. Kumarappan, J. of Opt. (2017), accepted.
[20] C. M. Maharjan, Ph.D. thesis, Kansas State University (2007).
[21] J. Ullrich, R. Moshammer, R. Dörner, O. Jagutzki, V. Mergel, H. Schmidt-Böcking, and L. Spielberger, Journal of Physics B: Atomic, Molecular and Optical Physics **30**, 2917 (1997).

[22] R. Dörner, V. Mergel, O. Jagutzki, L. Spielberger, J. Ullrich, R. Moshammer, and H. Schmidt-Böcking, Physics Reports **330**, 95 (2000).

[23] J. Ullrich, R. Moshammer, A. Dorn, R. Dörner, L. P. H. Schmidt, and H. Schmidt-Böcking, Reports on Progress in Physics **66**, 1463 (2003).

[24] This multiphoton ionization is assumed to be rapid, and the role of metastable autoionizing states negligible.

[25] E. Merzbacher, *Quantum Mechanics* (Wiley, 1998).

[26] The normal to the fragmentation plane is given by $\hat{\boldsymbol{z}} = \boldsymbol{p}_{\mathrm{CO,S}} \times \boldsymbol{p}_{\mathrm{CO}} \,/\, |\, \boldsymbol{p}_{\mathrm{CO,S}} \times \boldsymbol{p}_{\mathrm{CO}} \,|$, and $\hat{\boldsymbol{y}} = \boldsymbol{p}_{\mathrm{CO}} \,/\, |\, \boldsymbol{p}_{\mathrm{CO}} \,|$.

[27] C. D. Lin, Phys. Rep. **257**, 1 (1995).

[28] Y. Wang, Ph.D. thesis, Kansas State University (2010).

[29] The sensitivity of the $N(\theta_{\mathrm{CO,S}})$ distribution to the J states composing the rotational wavepacket and their lifetimes is under investigation.

[30] T. Severt, J. Rajput, B. Berry, B. Jochim, P. Feizollah, B. Kaderiya, M. Zohrabi, U. Ablikim, F. Ziaee, Kanaka-Raju P., D. Rolles, A. Rudenko, K. D. Carnes, B. D. Esry, and I. Ben-Itzhak, Phys. Rev. A (2017), in preparation.

[31] A. Khan, L. C. Tribedi, and D. Misra, Phys. Rev. A **92**, 030701 (2015).

[32] S. Yan, X. L. Zhu, P. Zhang, X. Ma, W. T. Feng, Y. Gao, S. Xu, Q. S. Zhao, S. F. Zhang, D. L. Guo, D. M. Zhao, R. T. Zhang, Z. K. Huang, H. B. Wang, and X. J. Zhang, Phys. Rev. A **94**, 032708 (2016).

[33] T. Šedivcová, P. R. Žďánská, V. Špirko, and J. Fišer, J. Chem. Phys. **124**, 214303 (2006).

[34] A. K. Edwards, R. M. Wood, and M. F. Steuer, Phys. Rev. A **16**, 1385 (1977).

[35] D. Mathur, Physics Reports **391**, 1 (2004), and references therein.

[36] M. Lundqvist, P. Baltzer, D. Edvardsson, L. Karlsson, and B. Wannberg, Phys. Rev. Lett. **75**, 1058 (1995).

[37] G. Dawber, A. G. McConkey, L. Avaldi, M. A. MacDonald, G. C. King, and R. I. Hall, J. Phys. B **27**, 2191 (1994).

[38] M. Hochlaf, R. I. Hall, F. Penent, H. Kjeldsen, P. Lablanquie, M. Lavollée, and J. H. D. Eland, Chem. Phys. **207**, 159 (1996).

[39] E. Y. Sidky and I. Ben-Itzhak, Phys. Rev. A **60**, 3586 (1999).

[40] B. Jochim, R. Erdwien, Y. Malakar, T. Severt, B. Berry, P. Feizollah, J. Rajput, B. Kaderiya, W. L. Pearson, K. D. Carnes, A. Rudenko, and I. Ben-Itzhak, New J. Phys. **19**, 103006 (2017).

[41] T. Šedivcová-Uhlková, P. R. Kaprálová-Žďánská, and V. Špirko, International Journal of Quantum Chemistry **107**, 2654 (2007).

[42] F. Mrugała, J. Chem. Phys. **129**, 064314 (2008).

[43] J. P. Bouhnik, I. Gertner, B. Rosner, Z. Amitay, O. Heber, D. Zajfman, E. Y. Sidky, and I. Ben-Itzhak, Phys. Rev. A **63**, 032509 (2001).

[44] A small correction due to the dips around $\theta_{\mathrm{CO,S}} = 0$ and 180 degrees is needed as detailed in Ref. [30].

[45] W. Kedzierski, J. Borbely, and J. W. McConkey, Journal of Physics B: Atomic, Molecular and Optical Physics **34**, 4027 (2001).